Redox Biology 38 (2021) 101783

Contents lists available at ScienceDirect

Redox Biology

journal homepage: www.elsevier.com/locate/redox

Research Paper

Perinatal inflammation alters histone 3 and histone 4 methylation patterns: Effects of MiR-29b supplementation

Sophia S. Sugar [a], Kathryn M. Heyob [a], Xinwei Cheng [b], Robert J. Lee [b], Lynette K. Rogers [a,c,*]

[a] Center for Perinatal Research, Abigail Wexner Research Institute at Nationwide Children's Hospital, USA
[b] College of Pharmacy, The Ohio State University, USA
[c] College of Medicine, The Ohio State University, Columbus, OH, USA

ARTICLE INFO

Keywords:
Hyperoxia
Lung injury
Methylation
Histone
microRNA

ABSTRACT

Preterm birth is still a major health problem and maternal inflammation has been shown to play a role. The combination of maternal inflammation and neonatal hyperoxia contributes to epigenetic changes that influence gene expression and the development of bronchopulmonary dysplasia (BPD). We have previously demonstrated suppression of miR-29b and increases in DNA methylation in infants with severe BPD and in our mouse model of maternal inflammation and neonatal hyperoxia exposure. The present studies further explored epigenetic changes in the murine model to include histone methylation. We identified a global suppression of histone methylation in exposed mice and validated decreases in expression in well-defined histone modifications, specifically H3K4me3, H3K27me3, H3K36me2, H3K79me2, and H4K20me3. We further tested the hypothesis that restoration of miR-29b expression would restore the histone methylation marks. Using lipid nanoparticle delivery of miR-29b, partial to full methylation was reestablished for H3K4me3, H3K27me3, and H4K20me3; all trimethylation marks. To identify the causes of decreased methylation in exposed mice, we measured commonly identified methylases and demethylases. We found a decreased expression of SUV40H2, a methylase primarily associated with H4K20me3. Further studies are needed to identify the causes for the decreased global histone methylation and potential therapeutic opportunities.

1. Background

Maternal inflammation is commonly associated with preterm birth [1,2]. Extremely preterm (<28 weeks gestation) infants are more likely to require respiratory support, which often includes mechanical ventilation and/or oxygen therapy [3]. The resulting oxidative lung injury and inflammation can develop into chronic lung disease or bronchopulmonary dysplasia (BPD) [4,5]. Subtle maternal inflammation, such as periodontal or urinary tract infections are thought to play a role in idiopathic preterm birth [6]. Our overarching hypothesis is that this subtle inflammation may predispose the infant for exacerbated responses to interventions such as hyperoxia and may be the underlying cause development of severe BPD. We and others have previously reported an early life suppression in pulmonary microRNA(miR)-29b in those infants that later develop BPD [7–9].

Systemic maternal inflammation can be mimicked through lipopolysaccharide (LPS) administration in animal models. This, in combination with neonatal hyperoxic exposure (LPS/O_2), induces production of reactive oxygen species and oxidative stress which in turn injures the lung, activates profibrotic pathways, impairs alveolarization, and diminishes lung function, mimicing the morbidities observed in preterm infants that develop severe BPD [10,11]. Our earlier work using this double-hit murine model indicated that miR-29 levels were accordingly suppressed and that restoration of miR-29b in newborn mice using adeno-associated viral (AAV) delivery improved alveolarization and prevented aberrant expression of matrix proteins in the developing lung [12]. Additionally, DNA methylation was substantially increased in both human tissues from infants that developed BPD and in our LPS/O_2 mouse model [7,13]. While AAV is not likely to be an accepted vehicle for therapeutics in preterm infants, these studies investigate the use of a LNP (lipid nano-particle) delivery system.

MiRs can regulate gene expression as well as coordinate other epigenetic mechanisms. Some miRs modulate chromatin structure and gene transcription by regulating DNA methylation and histone post-translational modifications (PTMs) [14,15]. Histone proteins have

* Corresponding author. Professor of Pediatrics, The Ohio State University Principal Investigator, Center for Perinatal Research, The Abigail Wexner Research Institute at Nationwide Children's Hospital, 575 Children's Cross Road, Columbus, Ohio, USA.
E-mail address: lynette.rogers@nationwidechildrens.org (L.K. Rogers).

https://doi.org/10.1016/j.redox.2020.101783
Received 25 August 2020; Received in revised form 9 October 2020; Accepted 29 October 2020
Available online 7 November 2020

Abbreviations

AAV	adeno-associated virus
BPD	bronchopulmonary dysplasia
H3	Histone 3
H4	Histone 4
KDM	lysine demethylase
KMT	lysine methyltransferase
LNP	lipid nano-particle
LPS	lipopolysaccharide
miR	microRNA
PDGFα	platelet derived growth factor alpha
PDGFRα	platelet derived growth factor receptor alpha
PN	postnatal
PRMT	protein arginine methyltransferase
PTM	post-translational modification
MMP	matrix metalloproteinase
αSMA	alpha smooth muscle actin

positively charged regions that are exposed to the cellular environment and are subject to PTMs. Such PTMs as methylation, acetylation, and phosphorylation, among others, are key players in the regulation of transcriptional activity and are critical in response to inflammation [16–18]. In the case of methylation particularly, methyl groups are transferred from ado-methionine to either lysine or arginine residues on histone tails [16]. Specifically, histones can be mono-, di-, or trimethylated at arginine and lysine residues and the modifications are thought to play a role in RNA processing, transcriptional regulation, signal transduction, chromatin maintenance, and DNA repair [19,20]. Oxidative stress has been shown to alter histone methylation patterns in cigarette smoke exposure, metal toxicities, cancers, and endothelial cells from preeclamptic pregnancies [21–24].

The enzymes that catalyze arginine methylation are known as protein arginine methyltransferases, or PRMTs [17]. PRMT1 (Type I) is the most abundant form of PRMTs and is expressed in most tissues. It is the enzyme primarily responsible for asymmetrical dimethylation, for example arginine 3 on histone H4 (H4R3me2a), which activates gene transcription [17]. Conversely, PRMT5 (Type II) catalyzes symmetrical dimethylation of arginine 3 on histone H4 (H4R3me2s), repressing gene transcription [17,18,25].

Histone lysine methylations impart active or repressive transcription depending on their proximity to specific genes and methylation statuses. Of the more commonly studied histone modifications, H3K4, H3K36, and H3K79 methylations confer active transcription, while H3K9, H3K27, and H4K20 methylations are generally known for transcriptional repression and silenced chromatin states [26]. Further, histone lysine methylations interact with DNA methylation to regulate gene transcription, particularly H3K9me2/3 and H4K20me3, which are thus of particular interest [16]. The enzyme families that catalyze lysine methylation and demethylation are known as protein lysine methyltransferases (KMTs) and protein lysine demethylases (KDMs), respectively. Many KMTs have been linked to human diseases and have established substrate specificity. For example, in the KMT family, EHMT1/2 activity gives rise to H3K9me2, SUV420H1/2 to H4K20me3, NSD1/2 to H3K36me2, and DOT1L to all three states (mono-, di-, and tri-) of H3K79 methylation. Importantly, some KMTs are more liberal in catalyzing substrates and can give rise to multiple histone lysine proteins. Similarly, KDMs remove methyl groups from histones and the KDM4 family of proteins, for instance, can demethylate H3K9me2 and H3K9me3 in addition to H3K36me2 and H3K36me3 [26,27]. The current study utilized our well-established double-hit mouse model to simulate the pathophysiology observed in infants with severe BPD to explore the associated changes in histone methylation patterns. Secondly, we hypothesized that LNP restoration of miR-29b to the lungs of neonatal LPS/O_2 exposed pups would attenuate the aberrant histone methylation patterns.

2. Methods

Animal model. For these investigations, we used our well-established and characterized double-hit model [10,11,28,29]. All studies were approved by the Abigail Wexner Research Institute at Nationwide Children's Hospital IACUC (protocol #AR07-00028) and followed ARRIVE guidelines. Pregnant C3H/HeN mice were injected intraperitoneally with lipopolysaccharide (LPS) or an equal volume of saline on embryonic day sixteen (E16). After birth, the litters were mixed and one of the litters was placed in 85% oxygen for 14 days (LPS/O_2), while the corresponding control litter was maintained in room air (saline/RA). On postnatal day 3 (PN3), mouse pups were given a LNP construct containing miR-29b-eGFP (enhanced green fluorescence protein) or an empty control LNP intranasally. On postnatal day 14 or 28 (PN), the mice were euthanized, and mouse lung tissues were collected for analysis. No sex differences have been previously identified in lung injury or lung developmental deficits during early life in this model and was not observed in these studies. Consequently, equal numbers of males and females were used for each analysis and the results are shown as mixed. All analyses included at least 3 litters with no more than 1 male and 1 female from each litter.

Preparation and administration of lipid nanoparticles (LNPs) encapsulating miR-29b. . LNPs with a composition of 1,2-dioleyloxy-3-dimethylaminopropane (DODMA)/dioleoylphosphatidylcholine (DOPC)/cholesterol/1,2-Dimyristoyl-rac-glycero-3-methoxypolyethylene glycol-2000 (mPEG2000-DMG) (35/30/30/5 m/m) was used to encapsulate synthetic miR-29b oligonucleotide duplexes. Briefly, lipids are dissolved in ethanol and rapidly mixed with miR-29b in 10% sucrose and 20 mM sodium citrate buffer at pH 4.0 and an ethanol-to-buffer ratio of 1:3 (vol/vol) to form LNPs by electrostatic complexation and self-assembly. The LNPs were then dialyzed against PBS (pH 7.4) in a Spectrum Slide-A-Lyzer™ cassette (with MWCO of 20,000) to remove residual ethanol, and then sterile-filtered using a 0.45 μm filter and stored at 4 °C until use. LNPs were characterized by size, zeta potential, and colloidal stability. The mean particle diameter and zeta potential of a typical LNP preparation were 135 nm (z-average) and 5.7 mV, respectively, determined on a Zetasizer Nano instrument by dynamic light scattering. Encapsulation of miR-29b was confirmed by agarose gel-electrophoresis that showed the absence of a free miRNA band. The LNPs were found to be stable at 4 °C for at least 3 weeks with less than 10% change in mean particle diameter. These particles were administered intranasally. Delivery was confirmed by fluorescence imaging and measuring changes in the expression of matrix proteins. Mouse pups were treated with either empty lipid nanoparticles (LNPs) or LNPs containing miR-29b-eGFP at PN3. LNP dosing was set at 2.9 μg RNA/mouse. After accounting for dilutions, this was administered as 3–5 μL liquid per dose per pup. Mice were held by the nape of the neck with the upper body stabilized, which allowed for micropipetting of the LNPs into the nostrils. Only 1–2 μL were pipetted at a time to ensure that the mouse inhaled the dosed liquid in its entirety. Pups were then held upright for 2–3 more minutes before finally being returned to their respective cages. The success of the administration was assessed by euthanizing pups 3–4 days after administration, inflation fixing with OTC, and freezing the lung tissues. Lungs were sectioned and viewed under a fluorescent microscope to visualize the labeled miR-29b-eGFP particles (Fig. 1A).

Morphometric analysis of lung tissue. Mice were anesthetized at PN28 and the left lung was inflation fixed at 25 cm of H_2O. Following paraffin embedding, tissue sections (5 μm) were cut and slides stained with hematoxylin and eosin (H&E) for morphometric measurements as previously described [30]. Five images per animal were analyzed and averaged using digital image analysis software (Image-Pro® Plus 6.3; Media Cybernetics, Silver Spring, MD). Additionally, the air space septal

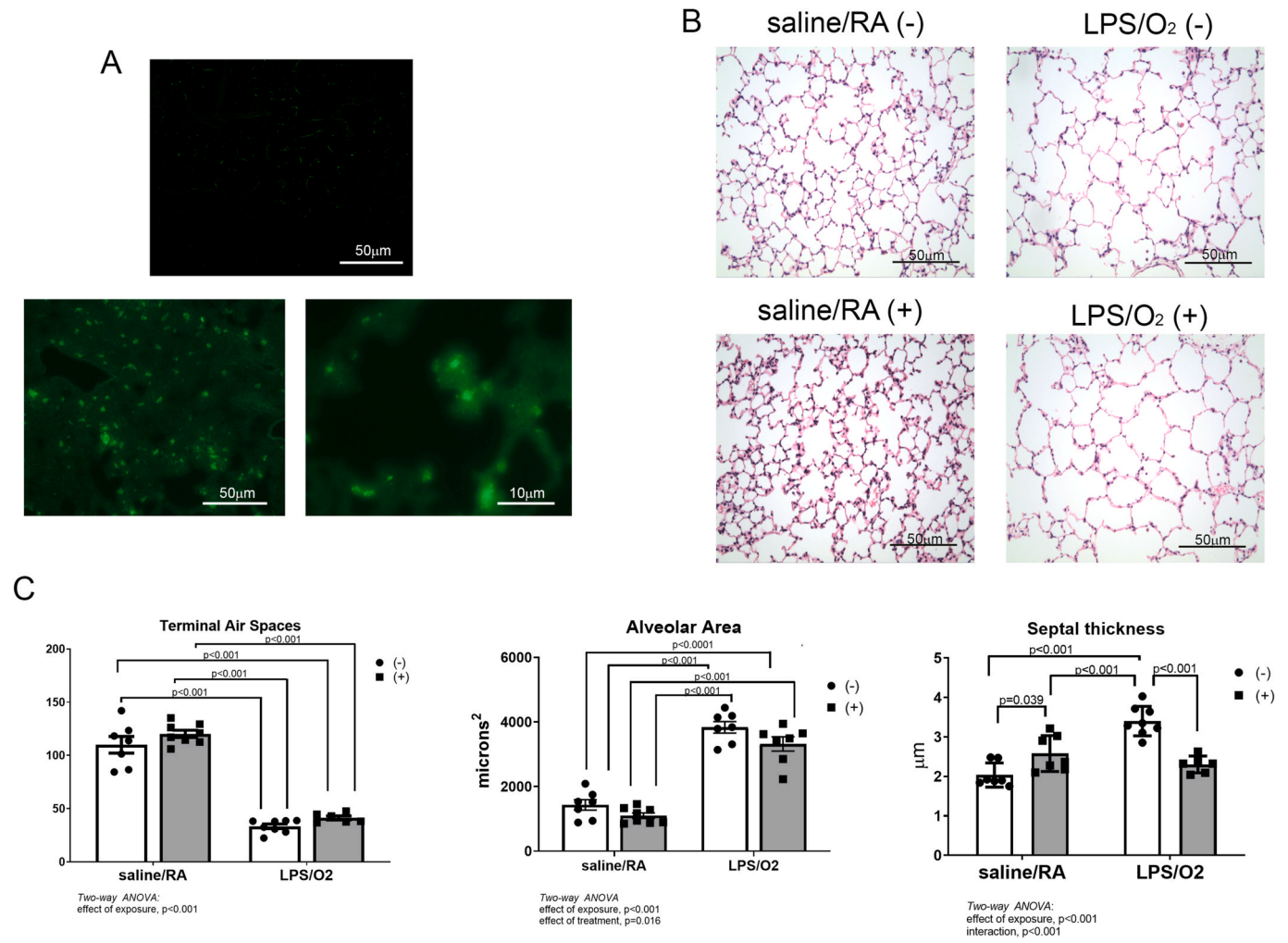

Fig. 1. LNP-miR-29b expression and morphometric analysis in lung tissues. Mice were exposed to saline/RA or LPS/O_2 after birth and treated with an LNP construct containing miR-29b-eGFP (enhanced green fluorescence protein) (+) or an empty LNP (-) intranasally at PN3. A: Pups were euthanized at PN6 and frozen sections prepared. Lung sections were viewed by fluorescence microscopy to visualize the labeled miR-29b-eGFP particles. Top photo is of non-LNP control, bottom photos were taken at × 100 (left) and × 400 (right). B: Mice were anesthetized at PN28. Formalin-fixed lung tissue sections were stained with hematoxylin-eosin and morphometric analyses were performed using Image-Pro Plus software. Photomicrographs were taken at × 100. C: Data were analyzed by two-way ANOVA to identify the effects of saline/RA or LPS/O_2 exposure and of miR-29b (-) or (+) treatment as indicated on the graph. Tukey's post-hoc analysis was used to determine significant differences between groups; $n = 7–8$. (For interpretation of the references to color in this figure legend, the reader is referred to the Web version of this article.)

wall thickness was measured randomly in five individually intact alveoli per image by manually identifying the septal wall edges and measuring the width.

Western blot analysis. Lung tissues from mice at PN28 were lysed via bead homogenization. Proteins were separated on 10% SDS-polyacrylamide gels and transferred to polyvinylidene fluoride membranes. The membranes were then stained with Ponceau S or 1X naphthol stain and quantified for normalization purposes. After blocking, membranes were probed with antibodies to αSMA (Sigma #A2547), MMP-9 (Abcam #ab119906), PDGFα (ABBiotech #250814) and PDGFRα (Cell Signaling #3164s) to assess changes in matrix proteins and PRMT1 (Cell Signaling #2449) and PRMT5 (Cell Signaling #2252) to assess arginine methyltransferases. Blots were developed using enhanced chemiluminescence (ECL) and ChemiDoc Imaging. Using Image Lab software (v 5.2.1) (BioRad, Hercules, CA), protein levels were quantified by densitometry. Quantifications for αSMA were normalized to β-actin (Abcam #ab6276). Remaining quantifications were normalized to total protein determined by Ponceau S staining for PRMT1, PRMT5 and PDGFα and naphthol staining for MMP and PDGFRα. We have previously reported validation of the use of total protein as a normalizer for Western blot analyses [31]. Images of the non-cropped gels are available in Supplemental Figs. 2 and 3.

Western blot analysis of histone modifications. Lung tissues from mice at PN28 were obtained and lysed via bead homogenization in a buffer (10 mM tris hydrochloride, 2.5 mM magnesium chloride, 0.5 mM calcium chloride, pH = 7.6). Then, 80 units of DNase was added per 100 μL lung homogenate. Samples were incubated at 37 °C for 10 min and DNase activity was stopped with 10 μL 0.5 M EDTA. Samples were separated on 15% SDS-polyacrylamide gels and transferred to polyvinylidene fluoride membranes. The membranes were then stained with 1X naphthol. After blocking, membranes were probed with antibodies to histone 4 arginine 3 dimethyl symmetric (H4R3me2s; Active Motif #61187) and histone 4 arginine 3 dimethyl asymmetric (H4R3me2a; Active Motif #39705). Blots were developed using enhanced chemiluminescence (ECL) and ChemiDoc Imaging. Using ImageQuantTL software, protein levels were quantified by densitometry. Quantifications were normalized to total protein determined via naphthol staining.

Histone purification. To extract total histone samples from lung tissues, the EpiQuik Total Histone Extraction Kit was used according to the manufacturer's protocol (Epigentek). Briefly, frozen lung tissues from

mice at PN28 were weighed, homogenized via Dounce homogenizer in 1X prelysis buffer, and centrifuged at 10,000 rpm for 1 min at 4 °C. After supernatant was removed, pellets were resuspended in 100 μL lysis buffer and incubated on ice for 30 min. Samples were centrifuged at 12,000 rpm for 5 min at 4 °C. Balance-dithiothreitol (DTT) buffer was added to each supernatant. Histone protein concentrations were measured by Bradford assay using a BSA standard.

Histone modification arrays. Multiple histone modifications on H3 and H4 were assessed in PN28 mouse lungs exposed to saline/RA or LPS/O_2 using the EpiQuik Histone H3 (and H4) Modification Multiplex Assay Kit (colorimetric) according to the manufacturer's instructions (Epigentek, Farmingdale, NY). In brief, histone extracts, prepared as described above, were used to determine the histone H3 and H4 modifications at specific sites. Respective capture antibodies were coated in strip wells and detected with a detection antibody. Data were obtained via microplate reader and OD values were measured at 450 nm wavelength. H3 and H4 modifications were calculated following the manufacturer's instructions.

Quantification of individual histone modifications. Levels of individual lysine histone modifications were quantified using commercial EpiQuik Global Histone Quantification Kits (colorimetric) for H3K4me3, H3K9me2, H3K27me3, H3K36me2, H3K79me2, and H4K20me3 (Epigentek). In these ELISA-based assays, methylated histones were captured with their respective, specific antibodies and measured using a detection antibody and color developer reagent. Lung tissues were obtained from mice at PN28 and histone extracts were prepared as described above. One hundred ng histone proteins were used for the assay and absorbance was read at 450 nm. Quantifications were calculated using a standard curve per the manufacturer's protocol.

PCR analyses of histone lysine methylases and demethylases. Expression levels of histone lysine demethylases KDM1A and KDM4(A-C), and histone lysine methylases EHMT1/2, SUV420H1/2, DOT1L, and NSD1/2 were measured via RTPCR. Pups were euthanized at PN14, lung tissues were harvested and homogenized via sonication. RNA was isolated by Trizol extraction followed by purification using Qiagen RNeasy Mini Kit and protocol. RNA was then reverse transcribed using the Maxima First-Strand cDNA Synthesis Kit (Thermo Scientific). Quantitative real-time PCR with SYBR green master mix (Thermo Scientific) was performed using an Eppendorf Realplex Master Cycler and custom DNA primers (Table 1).

Statistics. Two-way ANOVA or *t*-test was performed using GraphPad Prism version 8.0.0 for Windows (GraphPad Software, San Diego, California USA). Effects or interactions were determined between exposure variables, saline/RA or LPS/O_2, and treatment variables, miR-29b (+) or miR-29b (-). Tukey's post hoc analyses were performed to determine differences between individual groups. Data are expressed as means ± SEM and *p*-value results are indicated in the figures.

3. Results

Morphometric analysis and fluorescence imaging. Fluorescence imaging of lung tissue obtained 3–4 days after LNP delivery indicated that LNP-miR-29b reached the distal lung (Fig. 1A and Supplemental Fig. 1). Lung growth and development were assessed using morphometric analyses. LNP-miR-29b treatment did not result in significantly improved lung alveolarization (Fig. 1B and C). LNP-miR-29b treatment did normalize the aberrant increase in septal thickness (Fig. 1C) similar to AAV administration of miR-29b but in a more therapeutically relevant vehicle [12]. Since LNPs fuse with cell membranes to deliver their cargo, they are quickly phagocytosed and no fluorescence was observed after 7 days.

Western blot analysis of matrix proteins. Increases in αSMA and MMP-9 proteins contribute to changes in the composition and structure of the lung matrix. Exposure to LPS/O_2 significantly increased pulmonary protein levels of αSMA and MMP-9 (Fig. 2A and B). These elevations were attenuated with LNP-miR-29 (+) treatment. Exposure to LPS/O_2 decreased pulmonary protein levels of PDGFα and PDGFRα, indicating decreased expression of proteins essential for septal formation and alveolarization. Treatment with LNP-miR-29b (+) restored these important signaling proteins to control levels (Fig. 2C and D). Taken in combination, these data suggest that LNP-miR-29b supplementation in LPS/O_2-exposed mice pups attenuates pulmonary interstitial matrix changes and promotes fibroblast signaling.

Western blot analysis of PRMTs and histone arginine modifications. Protein levels of PRMT1 and PRMT5 in whole lung homogenates and their respective arginine methylation products, H4R3me2a and H4R3me2s, were measured by Western blot. Mice exposed to LPS/O_2 demonstrated significantly lower protein levels of PRMT1 but PRMT5, while trending lower, was not different than in the saline/RA mice (Fig. 3). In contrast, this decrease in PRMT1 protein did not result in changes in H4R3me2a, however, levels of H4R3me2s were lower in the exposed mice than in controls. This observed decrease in PRMT1 was attenuated with the intranasal treatment of LNP-miR-29b (+) (Fig. 3). Of note, the levels of PRMT5 after miR-29b treatment were greater than the saline/RA controls and did not result in an increase in H4R3me2s. These data suggest that LPS/O_2 exposure suppresses expression of PRMT1 and H4R3me2s, and the suppression of PRMT1 is partially attenuated by LNP-miR-29b supplementation.

Histone lysine modifications. To investigate histone lysine methylation, we performed histone 3 and histone 4 lysine methylation arrays (Fig. 4). Overall, most of the tested lysine methylations were decreased in the mice exposed to LPS/O_2 compared to saline/RA controls. The notable exception, however, was H3K79me2, which showed increased lysine methylation in LPS/O_2 mice (Fig. 4). We subsequently performed individual ELISAs for specific well-characterized lysine residues. We observed lower levels of lysine methylation at H3K4me3, H3K36me2,

Table 1
Primer sequences for PCR analyses.

Target	Forward Primer (5' → 3')	Reverse Primer (5' → 3')
KDM1A	GTGGTGTTATGCTTTGACCGT	GCTGCCAAAAATCCCTTTGAGA
KDM4A Variant 1	GACATAGTGAGTCAGGACTGTCT	GGCCACAAACTTAGCCCCATA
KDM4A Variant 2	TAATGTCTGAAAGCGGCTTCTG	TTCTGTTTGGAAACTGACCAGG
KDM4B	AGGGACTTCAACAGATATGTGGC	GATGTCATCATACGTCTGCCG
KDM4C	TGGAGAGTCCCCTAAATCCCA	CCTTGGCAAGACCTGCTCG
EHMT1	GAACAGGAGTCTCCCGACAC	GGGCTGTCAGTCTTCCCTC
EHMT2	GAAGTCGAAGCTCTAGCTGAAC	TGAGGAACCCACACCATTCAC
NSD1	TCCGGTGAATTTAGATGCCTCC	CGGTAACTGCATAGTACACCCA
NSD2	TGCCAAAAAGGAGTACGTGTG	CTTCGGGAAAGTCCAAGGCA
SUV420H1	ACTAGCGCCTTTCCTTCGAG	GCCGAAATCTCACAGGATTGTTG
SUV420H2	GCAGAGCTGCGTGAAGAGG	ACAGGCAGTATTCCCATCTGA
DOT1L	CAACTGCAAACATCACTACGGA	TCACCTCGTTCCAGTGTGTAT

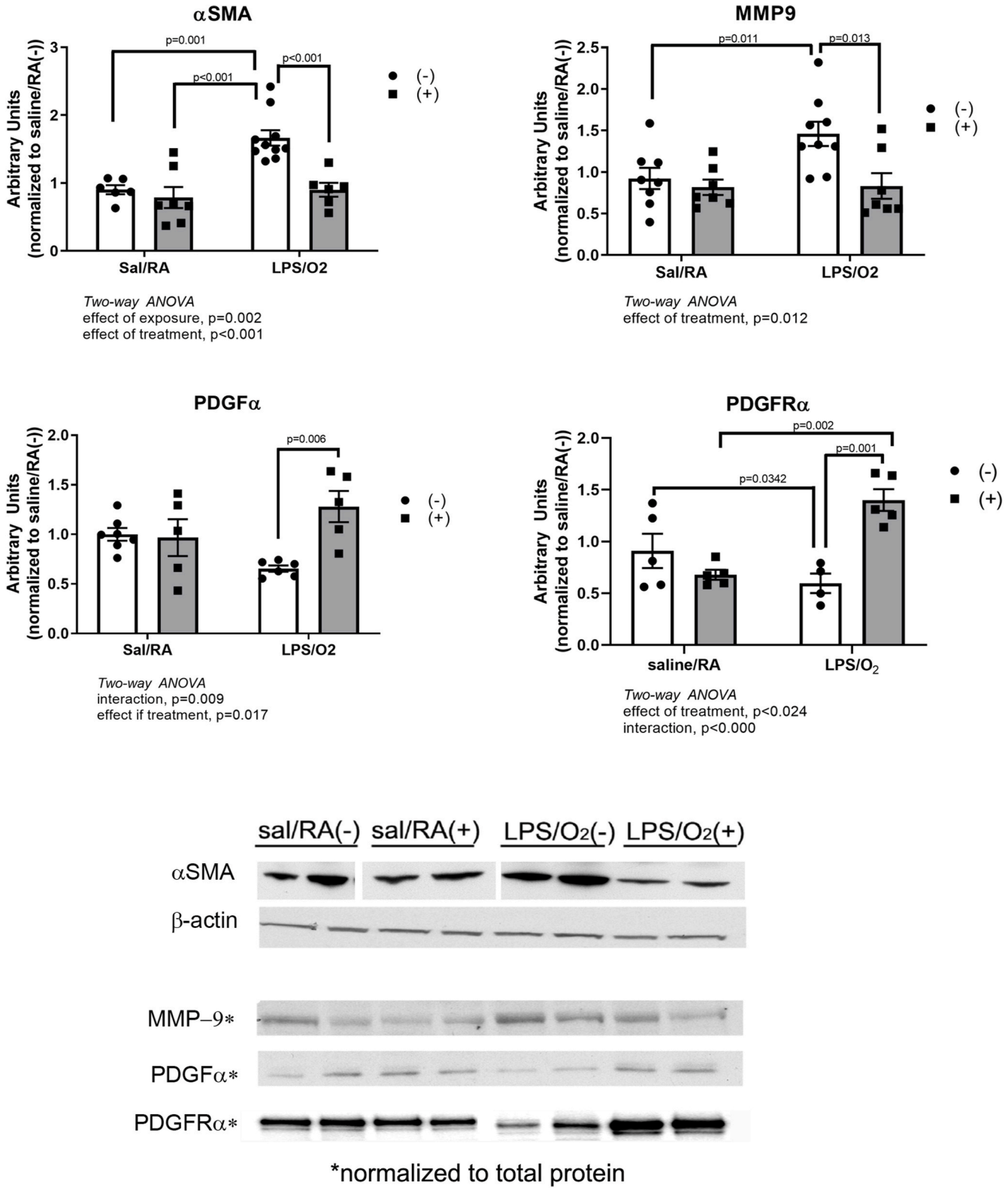

Fig. 2. Western blot analysis of matrix proteins. Lung tissues were harvested at PN28 to assess levels of matrix remodeling proteins, αSMA (A) and MMP-9 (B), and pulmonary signaling proteins, PDGFα (C) and its cognate receptor PDGFRα (D), via Western blot. Data were quantified by densitometry and analyzed by two-way ANOVA with Tukey's post-hoc; $n = 6–8$.

H3K79me2, and H4K20me3 in the LPS/O_2-exposed mice compared to saline/RA controls (Fig. 5). These decreases were partially or fully restored with miR-29b treatment, specifically, H3K4me3, H3K27me3, and H4K20me3, all trimethylation marks. There were no differences in H3K9me2 levels.

Lysine methylases and demethylases. Decreases in lysine methylation could be caused by lower activities of methylases or higher activities of demethylases. To address this issue, we chose representative lysine

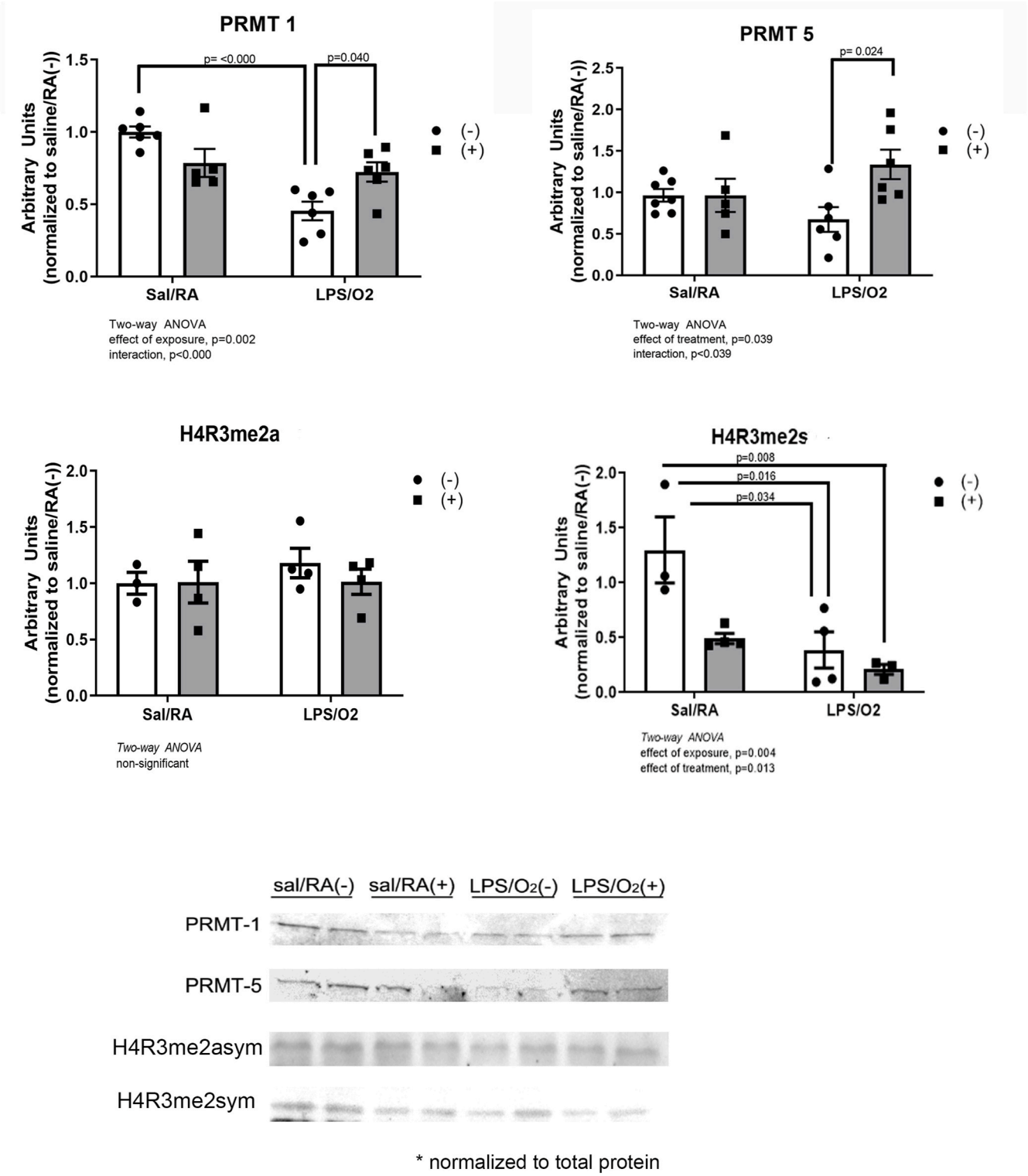

Fig. 3. Western blot analysis of protein arginine methyltransferases and histone methylation. Protein levels of PRMT1 and PRMT5 and their respective arginine methylation products, H4R3me2a and H4R3me2s, were measured by Western blot analysis in whole lung tissue homogenates at PN28. Data were quantified by densitometry and analyzed by two-way ANOVA with Tukey's post-hoc; $n = 4–7$.

methylases and demethylases and measured their expression levels by PCR at day 14, the time point for removal from oxygen,. The KDM family catalyzes lysine demethylation and the enzymes were chosen because of their characterization in the lung. We observed no differences in KDM4A (variant 1 or 2), KDM4C or KDM1A (Fig. 6A). We did, however, observe a decrease in KDM4B which is contrary to our hypothesis. We also measured lysine methylases. We observed no differences in EMHT1/2, NSD1/2, DOT1L, or SUV420H1, but observed a decrease in SUV420H2 (Fig. 6B). To determine the persistence of the changes in methylase activity and the effects of miR-29b supplementation, we measured the expression of the methylase, SUV40H2, and demethylase, KDM4B, at 28 day following room air recovery. Expression levels of the two tested

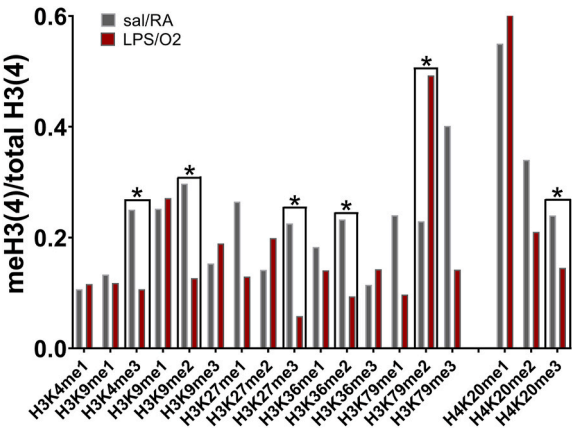

Fig. 4. Array of methylated lysine residues on histones 3 and 4. Histone proteins were isolated from lung tissue homogenates at PN28 using immunoprecipitation. Lysine methylation was measured using histone 3- and histone 4-specific modification arrays, n = 2–3. * indicated histone modifications validated by individual ELISA assays. * indicates the histone modifications analyzed by individual ELISAs.

enzymes had returned to normal in LPS/O_2 exposed mice at this time point. Interestingly, miR-29b supplementation caused a sustained decrease in both the expression of SUV40H1 and KDM4B (Fig. 6C).

4. Discussion

The epigenetic regulation of histone modifications and the enzymes that catalyze them is now understood to be of great pathological significance in many disease states associated with oxidative stress or inflammation [24]. Mutations and altered gene expressions of histone methyltransferases and demethylases are observed in cancers, developmental disorders, and other diseases [27]. Gains or losses of histone methylation marks can alter gene expression leading to either increased or decreased cell differentiation or proliferation [20,32]. Many studies have outlined the role of specific histone modifications in lung tumorigenesis and cell proliferation [14]. For example, dysregulation of H3K27 methylation has been found to be involved in tumor formation, metastasis, and increased proliferation. The NSD genes are known to function as oncogenes when overexpressed, associating H3K36me2 changes with cancer formation. SUV420H2, and subsequently H4K20me3 expression, was shown to be altered in lung and liver cancers [26].

Very little is known about changes in histone methylation patterns in BPD particularly. While a growing number of investigations are exploring changes in epigenetic signatures such as miRs and histone acetylation as possible contributing factors to BPD pathology, histone modifications in this disease have not been well-described. One study has linked PRMT5-induced regulation of Bone Morphogenic Protein 4 (BMP4) to lung branching morphogenesis in early lung development [33]. Others have identified interactions between DNMT3A and H4R3me2s in early embryogenesis [32]. We have previously reported substantial increases in DNMT expression and DNA methylation in our LPS/O_2 mouse model and in infants diagnosed with BPD, but the relationship between these DNA methylation increases and histone 3 and histone 4 methylation marks have not been investigated [7,13].

To further investigate the changes in histone methylation we incorporated our well-characterized LPS/O_2 model of severe BPD [10,11]. Our success with AAV-miR-29b treatment led us to further test miR-29b supplementation in normalizing aberrant histone modifications [12]. In these studies, we incorporated a safer and more practical delivery method, LNP-miR-29b. To ensure that we were delivering the LNPs to the distal lung, we observed fluorescence in lung tissue sections 3-4 days after dosing (Fig. 1A and Supplemental Fig. 1). We did not observe an

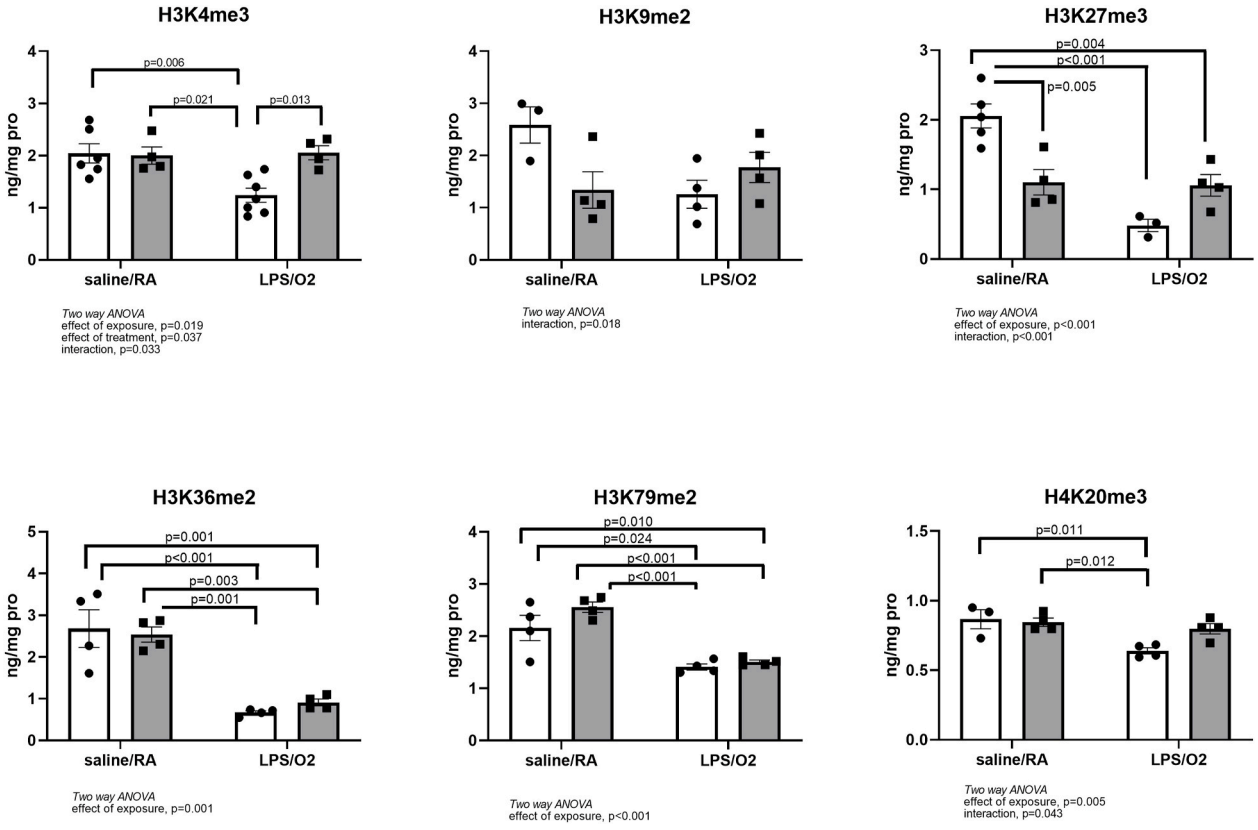

Fig. 5. ELISA analysis of individual methylated histone 3 and 4 lysine residues. Levels of H3K4me3, H3K9me2, H3K27me3, H3K36me2, H3K79me2, and H4K20me3 were assessed in lung tissue homogenates at PN28 by ELISA. Data were analyzed by two-way ANOVA and Tukey's post-hoc; $n = 4–7$.

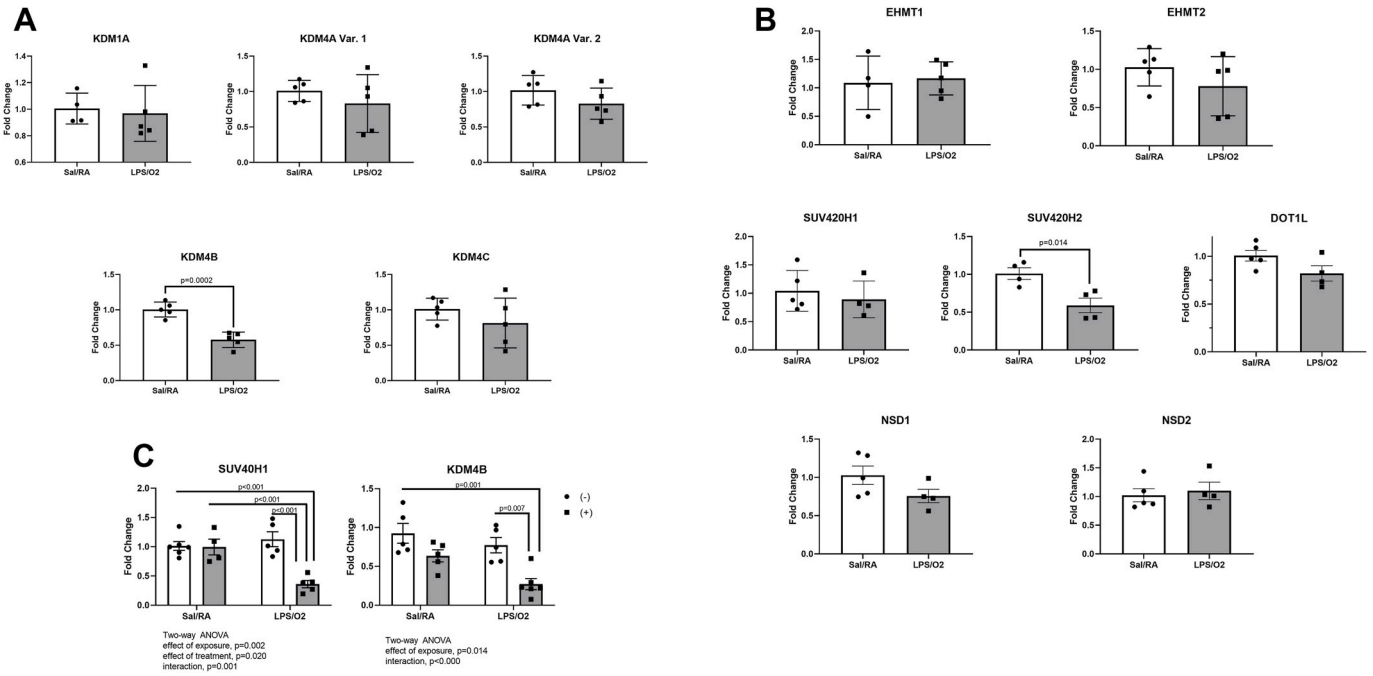

Fig. 6. PCR analysis of histone lysine methylases and demethylases. Mice were then euthanized at PN14 and lung RNA was isolated. Expression levels of lysine A) methylases (EHMT1/2, NSD1/2, SUV420H1/2, DOT1L) and B) demethylases (KDM4A variant 1 and 2, KDM1A, KDM4B, KDM4C) were measured via RTPCR analyses at day 14. C) At day 28, SUV40H1 and KDM4B were measured by PCR and the effects of miR-29b analyzed. Data were analyzed by *t*-test; $n = 4–5$ (A and B) and by two-way ANOVA n = 4–6 (C).

increase in alveolarization as previously observed, however, we did find normalization of septal thickness (Fig. 1B and C). We also measured the effects of LNP-miR-29b on matrix remodeling proteins, specifically αSMA and MMP-9 (Fig. 2A and B). Again, we observed normalization of these proteins to control levels in response to increased levels of miR-29b, similar to our previous studies [12]. To determine if miR-29b had any effect on an essential pathway involved with septal formation and alveolarization, we measured PDGFα and its cognate receptor PDGFRα (Fig. 2C and D). We observed modest decreases in these proteins with exposure to LPS/O_2 that were restored with miR-29b treatment.

PRMTs are a family of proteins that are classified according to the types of methylarginines they form. They can generate asymmetric dimethylarginine (Type I), symmetric dimethylarginine (Type II), or monomethylarginine (Type III). PRMT1 is responsible for 85% of arginine methylase activity and largely responsible for the formation of H4R3me2a which is involved in transcriptional activation [34]. Several common transcription factors have been shown to recruit PRMT1 to promoter regions, enhancing the assembly of transcriptional machinery [34,35]. PRMT5 also associates with promoter regions, specifically at CpG islands. Its role in DNA methylation is somewhat controversial but studies have indicated that H4R3me2s, the product of PRMT5 activity, associates with CpG islands and is likely involved in the recruitment of DNMT3A to DNA sequences to promote DNA methylation [34,36]. PRMT5 is also involved with cell cycle and the Swi/Snf complex, and the knockdown of PRMT5 results in slow growth and disruptions in the cell cycle [37].

We observed a decrease in PRMT1 protein expression in our LPS/O_2 exposed mice compared to saline/RA, indicating overall suppression of a transcriptional activator (Fig. 3). MiR-29b treatment was able to restore the PRMT1 protein to control levels. Interestingly, we observed no differences in H4R3me2a in the LPS/O_2 exposed mice, however, we observed a substantial decrease in H4R3me2s that was not affected by miR-29b treatment (Fig. 3). While difficult to interpret, these data imply that H4R3me2s recruitment to CpG islands is not likely a mechanism for reduced lung growth and decreased expression of the PDGF pathway in our model. One explanation is that the decrease in H4R3me2s is a result of an increase in demethylase activity, but further experiments are needed to investigate this hypothesis.

The mechanisms involved in methylation of lysine residues are less defined than those of arginine, with many targets on histone 3 and histone 4. Lysine can be mono-, di- and trimethylated and the results of our histone arrays indicate that most lysine methylation is decreased in our model. Others have also shown global decreases in lysine methylation marks with exposures that produce oxidative stress similar to that observed in the LPS/O_2 model [21,38,39]. The marked exception to this was H3K79me2, which indicated increased lysine methylation in the LPS/O_2-exposed mice (Fig. 4). When analyzed by an individual ELISA, the increase in H3K79me2 methylation did not replicate but was decreased as were the other H3 modifications. This discrepancy may be due to the low number of replicates (n = 2) used in the array. Notably, H3K79 is unlike other histone lysine methylations in that it occurs on the globular domain of histone H3 and is mediated by DOT1L, which lacks a SET domain. By contrast, other histone lysine methylations occur on histone tail domains and are catalyzed by SET domain-containing methylases [26].

Representative residues from histone 3 and one from histone 4 were also analyzed further. H3K4me3, H3K36me2, and H3K79me2 are transcription enhancers while H3K9me2, H3K27me3, and H4K20me3 are transcriptional silencers. Specifically, H4K20me3 is involved in genome integrity and chromatin packaging and maintenance [40,41]. We observed decreases in H3K4me3, H3K27me3, H3K36me2, H3K79me2, and H4K20me3 levels and a trend toward a decrease in H3K9me2 (Fig. 5). Further, levels of H3K4me3, H3K27me3, and H4K20me3 were restored with LNP-miR-29 treatment. We hypothesized that the observed decreases in lysine methylation could be due to decreases in methylase activity or increases in demethylase activity. To address this question, we chose several of the best-characterized lysine methylases and demethylases and measured their expression.

Many of the lysine methylases are promiscuous in their respective targets making identification of the enzyme responsible for a specific modification difficult. EHMT2 (G9a) both mono- and dimethylates

H3K9 and H3K27 and is abundantly expressed in mammalian tissues, along with its close relative EHMT1 (G9a-like protein) [16]. Neither of these common methylases, nor NSD1/2 or DOT1L, were decreased in the tissues obtained from LPS/O_2 mice (Fig. 6A). Additionally, SUV420H1/2 methylates H4K20me further to H4K20me2 and H4K20me3. They are both associated with heterochromatin and telomere maintenance, but only SUV420H2 has been found to play a role in lung cancers [26]. This is notable because no difference in SUV420H1 levels was measured but a significant decrease in SUV420H2 was observed in LPS/O_2 mice (Fig. 6B). This would support the hypothesis that the observed decrease in lysine methylation may due to decreases in specific lysine methyltransferase expression and activity.

Intriguingly, H4K20 methylation is regulated by a histone *trans*-tail mechanism and undergoes crosstalk with H3K9. SUV420H2 interacts with HP1 (heterochromatin protein 1), which recognizes H3K9 methylation. Thus, decreased levels of H3K9 methylation or HP1 protein can cause decreased heterochromatic targeting of SUV420H2 and a global reduction in H4K20me3. Recent studies have suggested that H3K9 methylation acts upstream of H4K20me3 [26,42]. Accordingly, our findings showed decreased H4K20me3 and SUV420H2 levels and a trend towards decreased H3K9me2 expression (Figs. 5 and 6B).

Alternatively, we measured the expression of several lysine demethylases (KDMs). KDM1A is known to demethylate H3K4 and was not different between saline/RA and LPS/O_2 mice. We also analyzed several members of a large family of lysine demethylases, KDM4 [43]. KDM4A-C proteins are known to demethylate the di- and trimethylated forms of H3K9 and H3K36, and isoforms B and C are induced by hypoxia [43]. Of those measured, expression levels of only one was altered, KDM4B was decreased (Fig. 6A). This does not coincide with our hypothesis that lysine demethylase activities were increased and is likely due to some other mechanism.

The decreases in SUV40H1 and KDM4B were evident at day 14 (Fig. 6B), at the time of removal from oxygen exposure, but was no longer detected at day 28 after room air recovery (Fig. 6C). This finding implies that suppression of these enzymes is associated with oxygen exposure and that the methylations observed on H3 and H4 are developmentally programed to occur during early life. Furthermore, the miR-29b treatment in early life causes sustained decreases in the expression of these enzymes at day 28. This would indicate that the restoration of tri-methylated histones by miR-29b treatment is not a direct result of these two enzymes. The intricate regulation of histone methylation in the context of developmental inflammation is likely to be complex and to change over time with maturation and recovery from the inflammatory insult. The connections between miR-29 and lysine methyltransferases has not been previous reported but may provide an interesting twist on the cross-talk between different epigenetic marks and their effects on development.

Histone methylation has not been previously explored in the context of a BPD model. This study is limited in the scope of the histone modifications and the methylases and demethylases that could be analyzed. Also, the cell specificity of the histone modifications was not elucidated and the genes affected by these modifications were not defined. We did not conclusively identify the mechanisms responsible for the global decreases histone methylation after LPS/O_2 exposure and were also not able to identify the mechanism involved in the sustained decreases in H4R3me2s despite normalizing the PRMT expression by treating with miR-29b. We also failed to establish the relationship between our previously published observation of elevated DMNT expression and decrease histone methylation although we speculate that increased DNA methylation may silence transcription of essential histone methyltransferases in a targeted manner.

These studies were not designed to establish a cause and effect relationship, but it is likely that these global decreases in histone methylation are involved in the aberrant regulation of alveolarization in the context of hyperoxia. We did identify cross-talk between miR-29b and histone methylation and opened a new avenue for pre-clinical investigations. Further studies are required to tease out the suppression of specific methylases and determine if restoration of activity could be a viable therapeutic approach. Findings from this investigation will provide the groundwork for exploration and validation of these changes in other models and human infants.

Funding sources

This work was supported by the National Institutes of Health, Eunice Kennedy Shriver National Institute of Child Health & Human Development [3HD0880833].

Declaration of competing interest

The authors of this manuscript have no Conflict of Interest to disclose.

Appendix A. Supplementary data

Supplementary data to this article can be found online at https://doi.org/10.1016/j.redox.2020.101783.

References

[1] C.S. Buhimschi, et al., Characterization of RAGE, HMGB1, and S100beta in inflammation-induced preterm birth and fetal tissue injury, Am. J. Pathol. 175 (2009) 958–975, ajpath.2009.090156 [pii] 10.2353/ajpath.2009.090156.
[2] I.A. Buhimschi, et al., The receptor for advanced glycation end products (RAGE) system in women with intraamniotic infection and inflammation, Am. J. Obstet. Gynecol. 196 (2007) 181 e181–113. S0002-9378(06)01179-3 [pii]10.1016/j.ajog.2006.09.001.
[3] E. Baraldi, S. Carraro, M. Filippone, Bronchopulmonary dysplasia: definitions and long-term respiratory outcome, Early Hum. Dev. 85 (2009) S1–S3, https://doi.org/10.1016/j.earlhumdev.2009.08.002S0378-3782(09)00130-3 [pii].
[4] A. Greenough, Long term respiratory outcomes of very premature birth (<32 weeks), Semin. Fetal Neonatal Med. 17 (2012) 73–76, https://doi.org/10.1016/j.siny.2012.01.009S1744-165X(12)00010-8 [pii].
[5] B.J. Stoll, et al., Neonatal outcomes of extremely preterm infants from the NICHD Neonatal Research Network, Pediatrics 126 (2010) 443–456, https://doi.org/10.1542/peds.2009-2959peds.2009-2959 [pii].
[6] E.S. Green, P.C. Arck, Pathogenesis of preterm birth: bidirectional inflammation in mother and fetus, Semin. Immunopathol. (2020), https://doi.org/10.1007/s00281-020-00807-y.
[7] L.K. Rogers, et al., Attenuation of miR-17-92 cluster in bronchopulmonary dysplasia, Ann. Am. Thorac. Soc. 12 (2015) 1506–1513, https://doi.org/10.1513/AnnalsATS.201501-058OC.
[8] L. Cushing, et al., Disruption of miR-29 leads to aberrant differentiation of smooth muscle cells selectively associated with distal lung vasculature, PLoS Genet. 11 (2015), e1005238, https://doi.org/10.1371/journal.pgen.1005238.
[9] L. Cushing, et al., miR-29 is a major regulator of genes associated with pulmonary fibrosis, Am. J. Respir. Cell Mol. Biol. 45 (2011) 287–294, 2010-0323OC [pii] 10.1165/rcmb.2010-0323OC.
[10] M. Velten, et al., Prenatal inflammation exacerbates hyperoxia-induced functional and structural changes in adult mice, Am. J. Physiol. Regul. Integr. Comp. Physiol. 303 (2012) R279–R290, https://doi.org/10.1152/ajpregu.00029.2012ajpregu.00029.2012 [pii].
[11] M. Velten, K.M. Heyob, L.K. Rogers, S.E. Welty, Deficits in lung alveolarization and function after systemic maternal inflammation and neonatal hyperoxia exposure, J. Appl. Physiol. 108 (2010) 1347–1356, https://doi.org/10.1152/japplphysiol.01392.200901392.2009 [pii].
[12] S. Durrani-Kolarik, et al., miR-29b supplementation decreases expression of matrix proteins and improves alveolarization in mice exposed to maternal inflammation and neonatal hyperoxia, Am. J. Physiol. Lung Cell Mol. Physiol. 313 (2017) L339–L349, https://doi.org/10.1152/ajplung.00273.2016.
[13] M.E. Robbins, D. Dakhlallah, C.B. Marsh, L.K. Rogers, T.E. Tipple, Of mice and men: correlations between microRNA-17 approximately 92 cluster expression and promoter methylation in severe bronchopulmonary dysplasia, Am. J. Physiol. Lung Cell Mol. Physiol. 311 (2016) L981–L984, https://doi.org/10.1152/ajplung.00390.2016.
[14] M. Fabbri, et al., MicroRNA-29 family reverts aberrant methylation in lung cancer by targeting DNA methyltransferases 3A and 3B, Proc. Natl. Acad. Sci. U. S. A. 104 (2007) 15805–15810, https://doi.org/10.1073/pnas.0707628104.
[15] J. Dong, et al., MicroRNA-mRNA interactions in a murine model of hyperoxia-induced bronchopulmonary dysplasia, BMC Genom. 13 (2012) 204, https://doi.org/10.1186/1471-2164-13-2041471-2164-13-204 [pii].
[16] S.C. Dillon, X. Zhang, R.C. Trievel, X. Cheng, The SET-domain protein superfamily: protein lysine methyltransferases, Genome Biol. 6 (2005) 227, https://doi.org/10.1186/gb-2005-6-8-227.

[17] S. Jahan, J.R. Davie, Protein arginine methyltransferases (PRMTs): role in chromatin organization, Adv. Biol. Regul. 57 (2015) 173–184, https://doi.org/10.1016/j.jbior.2014.09.003.
[18] J.H. Kim, et al., The role of protein arginine methyltransferases in inflammatory responses, Mediat. Inflamm. (2016), 4028353, https://doi.org/10.1155/2016/4028353.
[19] F. Fuks, DNA methylation and histone modifications: teaming up to silence genes, Curr. Opin. Genet. Dev. 15 (2005) 490–495, https://doi.org/10.1016/j.gde.2005.08.002.
[20] A. Jeltsch, J. Broche, P. Bashtrykov, Molecular processes connecting DNA methylation patterns with DNA methyltransferases and histone modifications in mammalian genomes, Genes (Basel) 9 (2018), https://doi.org/10.3390/genes9110566.
[21] W. Sheng, et al., Upregulation of histone H3K9 methylation in fetal endothelial cells from preeclamptic pregnancies, J. Cell. Physiol. (2020), https://doi.org/10.1002/jcp.29970.
[22] I.K. Sundar, H. Yao, I. Rahman, Oxidative stress and chromatin remodeling in chronic obstructive pulmonary disease and smoking-related diseases, Antioxidants Redox Signal. 18 (2013) 1956–1971, https://doi.org/10.1089/ars.2012.4863.
[23] Y. Chervona, M. Costa, The control of histone methylation and gene expression by oxidative stress, hypoxia, and metals, Free Radic. Biol. Med. 53 (2012) 1041–1047, https://doi.org/10.1016/j.freeradbiomed.2012.07.020.
[24] Y. Niu, T.L. DesMarais, Z. Tong, Y. Yao, M. Costa, Oxidative stress alters global histone modification and DNA methylation, Free Radic. Biol. Med. 82 (2015) 22–28, https://doi.org/10.1016/j.freeradbiomed.2015.01.028.
[25] M. Girardot, et al., PRMT5-mediated histone H4 arginine-3 symmetrical dimethylation marks chromatin at G + C-rich regions of the mouse genome, Nucleic Acids Res. 42 (2014) 235–248, https://doi.org/10.1093/nar/gkt884.
[26] K. Hyun, J. Jeon, K. Park, J. Writing Kim, Erasing and reading histone lysine methylations, Exp. Mol. Med. 49 (2017) e324, https://doi.org/10.1038/emm.2017.11.
[27] D. Husmann, O. Gozani, Histone lysine methyltransferases in biology and disease, Nat. Struct. Mol. Biol. 26 (2019) 880–889, https://doi.org/10.1038/s41594-019-0298-7.
[28] M. Velten, et al., Adverse perinatal environment contributes to altered cardiac development and function, Am. J. Physiol. Heart Circ. Physiol. 306 (2014) H1334–H1340, https://doi.org/10.1152/ajpheart.00056.2014ajpheart.00056.2014 [pii].
[29] M. Velten, et al., Systemic maternal inflammation and neonatal hyperoxia induces remodeling and left ventricular dysfunction in mice, PLoS One 6 (2011), e24544, https://doi.org/10.1371/journal.pone.0024544.
[30] M.S. Park, et al., Altered expressions of fibroblast growth factor receptors and alveolarization in neonatal mice exposed to 85% oxygen, Pediatr. Res. 62 (2007) 652–657.
[31] K.M. Heyob, et al., Maternal high-fat diet alters lung development and function in the offspring, Am. J. Physiol. Lung Cell Mol. Physiol. 317 (2019) L167–L174, https://doi.org/10.1152/ajplung.00331.2018.
[32] A. Henckel, et al., Histone methylation is mechanistically linked to DNA methylation at imprinting control regions in mammals, Hum. Mol. Genet. 18 (2009) 3375–3383, https://doi.org/10.1093/hmg/ddp277.
[33] Q. Li, et al., Histone arginine methylation by Prmt5 is required for lung branching morphogenesis through repression of BMP signaling, J. Cell Sci. 131 (2018), https://doi.org/10.1242/jcs.217406.
[34] A. Di Lorenzo, M.T. Bedford, Histone arginine methylation, FEBS Lett. 585 (2011) 2024–2031, https://doi.org/10.1016/j.febslet.2010.11.010S0014-5793(10)00906-3 [pii].
[35] M.T. Bedford, S. Richard, Arginine methylation an emerging regulator of protein function, Mol. Cell. 18 (2005) 263–272, https://doi.org/10.1016/j.molcel.2005.04.003. S1097-2765(05)01247-5 [pii].
[36] Q. Zhao, et al., PRMT5-mediated methylation of histone H4R3 recruits DNMT3A, coupling histone and DNA methylation in gene silencing, Nat. Struct. Mol. Biol. 16 (2009) 304–311, https://doi.org/10.1038/nsmb.1568nsmb.1568 [pii].
[37] V. Karkhanis, Y.J. Hu, R.A. Baiocchi, A.N. Imbalzano, S. Sif, Versatility of PRMT5-induced methylation in growth control and development, Trends Biochem. Sci. 36 (2011) 633–641, https://doi.org/10.1016/j.tibs.2011.09.001S0968-0004(11)00143-5 [pii].
[38] S. Sunnaghatta Nagaraja, et al., Radiation-induced H3K9 tri-methylation in E-cadherin promoter during lung EMT: in vitro and in vivo approaches using vanillin, Free Radic. Res. (2020) 1–16, https://doi.org/10.1080/10715762.2020.1814274.
[39] Y.S. Ryu, et al., Particulate matter-induced senescence of skin keratinocytes involves oxidative stress-dependent epigenetic modifications, Exp. Mol. Med. 51 (2019) 1–14, https://doi.org/10.1038/s12276-019-0305-4.
[40] R. van Nuland, O. Gozani, Histone H4 lysine 20 (H4K20) methylation, expanding the signaling potential of the proteome one methyl moiety at a time, Mol. Cell. Proteomics 15 (2016) 755–764, https://doi.org/10.1074/mcp.R115.054742.
[41] M. Shoaib, et al., Histone H4K20 methylation mediated chromatin compaction threshold ensures genome integrity by limiting DNA replication licensing, Nat. Commun. 9 (2018) 3704, https://doi.org/10.1038/s41467-018-06066-8.
[42] S. Fioriniello, D. Marano, F. Fiorillo, M. D'Esposito, F. Della Ragione, Epigenetic factors that control pericentric heterochromatin organization in mammals, Genes (Basel) 11 (2020), https://doi.org/10.3390/genes11060595.
[43] R.M. Labbe, A. Holowatyj, Z.Q. Yang, Histone lysine demethylase (KDM) subfamily 4: structures, functions and therapeutic potential, Am. J. Transl. Res. 6 (2013) 1–15.